Supplementary Information for

Distributed direct air capture of carbon dioxide by synergistic water harvesting

Yongqiang Wang[1,2], Longbing Qu[1], Hui Ding[2*], Paul Webley[3*], Gang Kevin Li[1*]

[1]Department of Chemical Engineering, The University of Melbourne, Parkville, Victoria 3010, Australia.

[2]School of Environmental Science and Engineering, Tianjin University, Tianjin 300072, China.

[3]Department of Chemical and Biological Engineering, Monash University, Clayton, Victoria 3800, Australia.

*Correspondence: li.g@unimelb.edu.au (G.L.), paul.webley@monash.edu (P.W.), dinghui@tju.edu.cn (H.D.)

List of Supplementary Information:

1. Supplementary Methods.
2. Supplementary Figures 1-16.
3. Supplementary Table 1-4.
4. Supplementary References.

Supplementary Methods

Estimation of regeneration efficiency R for the vapor promoted desorption

To predict the performance of vapor promoted desorption at 1 bar, we initially focused on the impact of co-adsorbed water on the desorption temperature required to achieve a specific regeneration efficiency *R* (Supplementary Fig. 13). This investigation involved calculating the equilibrium loadings of adsorbed water and CO_2 in the column using water adsorption isotherms and CO_2 loading profiles obtained during DAC cycles (Supplementary Figs. 2 and 12). To achieve an equilibrium state, a minimum adsorption duration of 4 hours was performed to capture atmospheric CO_2 and water. Subsequently, we observed a linear correlation, as shown in Supplementary Fig. 13, between the required desorption temperature and the molar ratio of the equilibrium loading of adsorbed water to CO_2 (n_{water}/n_{CO2}) for vapor promoted desorption with a specific *R*.

This linear correlation in Supplementary Fig. 13 enables us to calculate the required n_{water}/n_{CO2} for reaching different *R* values at certain desorption temperatures and 1 bar. Then, the corresponding volume fraction of resin ($V_{f,resin}$) under different atmospheric humidities can be evaluated by Supplementary Equation 1.

$$V_{f,resin} = \frac{q_{water,silica}\rho_{silica}}{\left(q_{CO_2,resin}\rho_{resin}n_{water}/n_{CO_2} - q_{water,resin}\rho_{resin} + q_{water,silica}\rho_{silica}\right)} \quad (1)$$

where $q_{water,silica}$ and $q_{water,resin}$ (mmol g^{-1}) represent the equilibrium water loadings for silica gel and Lewatit resin at different relative humidities. ρ_{silica} and ρ_{resin} (g L^{-1}) are the packing densities of silica gel and Lewatit resin, respectively. To calculate the volume fraction of resin, the adsorption temperature is set at 28 °C. The equilibrium CO_2 adsorption capacity of Lewatit resin ($q_{CO_2,resin}$) is calculated using the isotherm model parameters (Supplementary Table 1) and the enhancement factor under different humidities (Supplementary Fig. 4). Then, the correlation between regeneration efficiency and given conditions (volume fraction of resin, desorption temperature, and relative humidity of feed air) is obtained and depicted in Fig. 4e.

We have also observed that the desorption temperatures were higher than the boiling point of water by no more than 20 °C, depending on the n_{water}/n_{CO2}, as shown in Supplementary Fig. 13. This relationship highlights the potential of operating VPD at lower temperatures by reducing the desorption pressure and also the water boiling point, allowing us to predict the corresponding *R* under vacuum conditions. To evaluate the regeneration performance at a moderate desorption pressure of 0.5 bar, three assumptions were considered:

1. The desorption kinetics were assumed to be unchanged compared with vapor promoted desorption at 1 bar.
2. A high regeneration efficiency (around 0.93) is still achievable under vacuum conditions with *in situ* vapor purge.
3. Based on the aforementioned two assumptions, it is assumed that the linear correlation observed in Supplementary Fig. 13 between ΔT and n_{water}/n_{CO2} at 1 bar remains valid under a moderate desorption pressure of 0.5 bar.

Thus, for achieving different *R* at 0.5 bar, the required desorption temperature under specific n_{water}/n_{CO2} can be calculated based on Supplementary Equation 2 and Supplementary Fig. 13,

with $T_{bp,\ 0.5\ bar}$ representing the boiling point of water at 0.5 bar. The performance of vapor promoted desorption at 0.5 bar can be evaluated using a similar approach as the one employed for predicting regeneration efficiency at 1 bar.

$$T_{de,0.5\ bar} = \Delta T + T_{bp,0.5bar} \quad (2)$$

Photothermal conversion efficiency and energy consumption of the solar-powered DAC prototype

To calculate the photothermal conversion efficiency of the solar-powered DAC prototype, temperature increases of an empty solar-heating column were measured under sunlight irradiation. The thermal energy ($Q_{thermal}$) converted from solar energy as well as the photothermal conversion efficiency (α) were calculated using Supplementary Equations 3-4,

$$Q_{thermal} = \alpha A \int_0^t I_{solar} dt = m_{tube} C_{tube} \Delta T_{tube} \quad (3)$$

$$\alpha = \frac{m_{tube} C_{tube} \Delta T_{tube}}{A \int_0^t I_{solar} dt} \quad (4)$$

where A is the projected area (0.05 m^2) of the black coating for receiving natural sunlight, I_{solar} is the solar flux, t is the solar irradiation time, m_{tube} refers to the mass of the solar-heating column (1.07 kg), C_{tube} is the heat capacity (500 J kg^{-1} K^{-1}) of the tube, ΔT_{tube} represents the temperature increase of the adsorption column during solar heating.

A parabolic concentrator was used to enhance the heating power of the photothermal DAC prototype. Fig. 5b shows the temperature increases of the adsorption column under natural and concentrated sunlight. The optical concentration ratio (σ) of the parabolic concentrator was determined by conducting solar heating experiments under concentrated sunlight and calculated using Supplementary Equation 5.

$$\sigma = \frac{m_{tube} C_{tube} \Delta T_{tube}}{\alpha A \int_0^t I_{solar} dt} \quad (5)$$

Using the temperature profiles in Fig. 5b, the overall photothermal conversion efficiency (α) of the solar heating column was determined to be 63.1%. The optical concentration ratio was measured and calculated to be 1.9. Subsequently, the heating powers (W) of the photothermal system under various solar intensities were calculated using Supplementary Equation 6.

$$W = \alpha \sigma A I_{solar} \quad (6)$$

For the solar-powered DAC system, the thermal energy for adsorbent regeneration (Q_{re}) was calculated based on the following equation,

$$Q_{re} = \sigma \alpha A \frac{\int_o^{t_{des}} I_{solar} dt}{m_{CO_2}} - \frac{m_{tube} C_{tube} \Delta T_{tube}}{m_{CO_2}} \quad (7)$$

where t_{des} is the desorption time, and m_{CO_2} is the mass of CO_2 collected under solar irradiation, ΔT_{tube} represents the temperature increase of the adsorption column in the desorption stage. Considering that reported energy consumption analyses typically focus on the energy used for heating the adsorbent and providing latent heat, this study subtracted the heat required for heating the adsorption column, to enable a meaningful comparison.

The energy consumption (Q_{re}) for sorbent regeneration can also be directly calculated based on the sensible heat (Q_s) required to increase the temperatures and the latent heat (Q_d) associated with CO_2 and water desorption, as illustrated by Supplementary Equation 8.

$$Q_{re} = \frac{Q_s + Q_d}{m_{CO_2}} \quad (8)$$

Q_s is computed using the following equation,

$$Q_s = \Delta T (m_{resin} C_{p,resin} + m_{silica} C_{silica} + m_{CO_2}^{(ads)} C_{p,CO_2} + m_{H_2O}^{(ads)} C_{p,H_2O}) \quad (9)$$

where ΔT signifies the sorbent temperature variation during the desorption process; m_{resin}, m_{silica}, $m_{CO_2}^{(ads)}$ and $m_{H_2O}^{(ads)}$ represent the masses of amine-grafted resin, silica gel, adsorbed CO_2 and water within the column, respectively; $C_{p,resin}$, $C_{p,silica}$, C_{p,CO_2} and C_{p,H_2O} denote the specific heat capacities of amine-grafted resin, silica gel, adsorbed CO_2 and water within the column, respectively.

Supplementary Equation 10 is employed to analyze latent heat, where Q_{des,CO_2} and Q_{des,H_2O} represent the heat required for CO_2 and water desorption, respectively; n_{CO_2} and n_{H_2O} represent the moles of collected CO_2 and water products during the desorption process, respectively; h_{des,CO_2} and h_{des,H_2O} are the heat of desorption for CO_2 and water, respectively. The parameters used for evaluating energy consumption are listed in Supplementary Table 2.

$$Q_d = Q_{des,CO_2} + Q_{des,H_2O} = n_{CO_2} h_{des,CO_2} + n_{H_2O} h_{des,H_2O} \quad (10)$$

Estimation of the total cost for the vapor-promoted DAC process

The total cost (c_{total}) of vapor-promoted DAC is analyzed based on a reported economic evaluation approach[1]. The calculation method is described in Supplementary Equation 11. The capital expenditures (c_{CAPEX}) are divided into plant costs (especially the cost for air contactor, c_{plant}) and sorbent costs ($c_{sorbent}$). The energy costs (c_{energy}) can be regarded as proxy for the operational expenditures (c_{OPEX}).

$$c_{total} = c_{CAPEX} + c_{OPEX} = c_{plant} + c_{sorbent} + c_{energy} \tag{11}$$

The plant cost can be calculated by Supplementary Equation 12.

$$c_{plant} = \frac{r_{ac}}{V_{f,resin} P_r a_p} \tag{12}$$

where r_{ac} signifies the air contactor cost per cubic meter, $V_{f,resin}$ is volume fraction of resin inside the column, P_r represent the CO_2 productivity based on the volume of resins, a_p is the lifetime of the plants.

As two adsorbents are used in vapor-promoted DAC, the sorbent cost includes the cost for two different materials.

$$c_{sorbent} = \frac{V_{f,resin} r_{resin} + (1 - V_{f,resin}) r_{silica}}{V_{f,resin} P_r a_s} \tag{13}$$

where r_{resin} and r_{silica} are CO_2 capture resin and silica gel costs per cubic meter, respectively. a_s is the lifetime of the sorbents.

For the evaluation of operational expenditures, the electricity cost for air blowers and thermal energy cost for sorbent regeneration constitute the total energy cost.

$$c_{energy} = c_{th} Q_{re} + c_{el} E_{blower} \tag{14}$$

where c_{th} and c_{el} are the heat price and electricity price, respectively. Q_{re} and E_{blower} are the energy consumption for regenerating sorbents in the desorption step and blowing air in the adsorption step, respectively.

The units and values of the parameters used for evaluating capture cost are listed in Supplementary Table 4.

Supplementary Figures

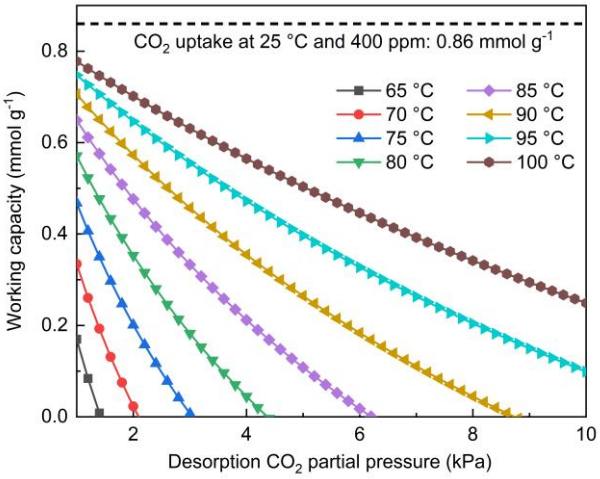

Supplementary Fig. 1. Calculated working capacity of VP OC 1065 under different desorption temperatures and CO_2 partial pressures. Adsorption conditions are fixed at 25 °C air and 400 ppm CO_2. The solid lines are guides to the eye. Source data are provided as a Source Data file.

Lewatit VP OC 1065 is a commercially available amine-functionalized resin and can be regarded as a benchmark for DAC studies[2]. CO_2 working capacities of the resin under different desorption temperatures and pressures were calculated using a reported dual site Langmuir isotherm model, as illustrated in Supplementary Table 1[3,4].

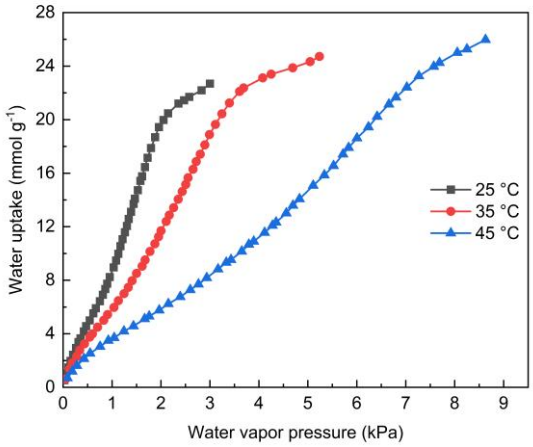

Supplementary Fig. 2. Water adsorption isotherms of silica gel at 25 °C, 35 °C, and 45 °C. The solid lines are guides to the eye. Source data are provided as a Source Data file.

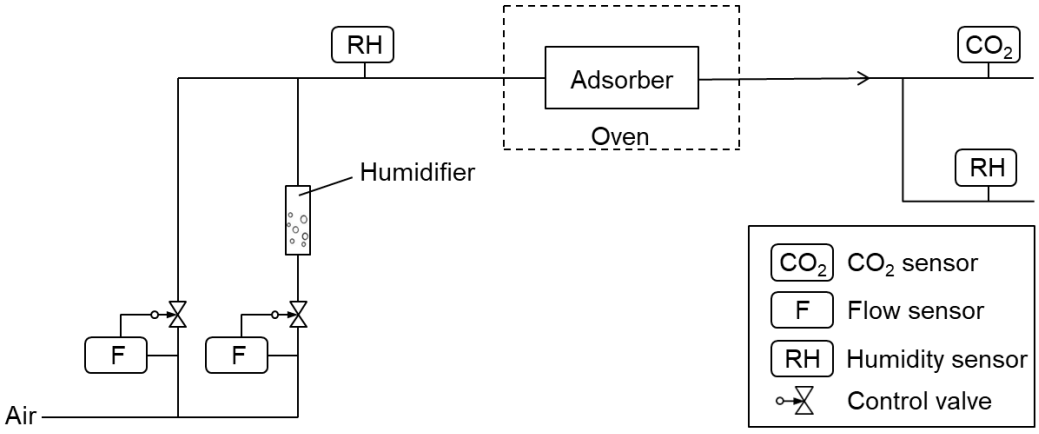

Supplementary Fig. 3. Scheme of the setup for breakthrough experiments.

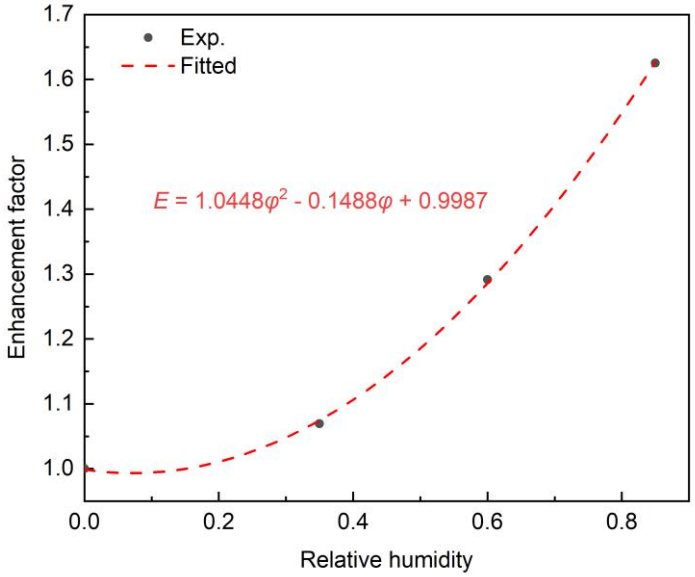

Supplementary Fig. 4. Enhancement factor (*E*) under different relative humidities (φ) for the amine-grafted resin at 28 °C and 410 ppm CO_2. The enhancement factor is defined as the ratio between CO_2 adsorption capacities under humid and dry conditions. The results are fitted by a polynomial equation. Source data are provided as a Source Data file.

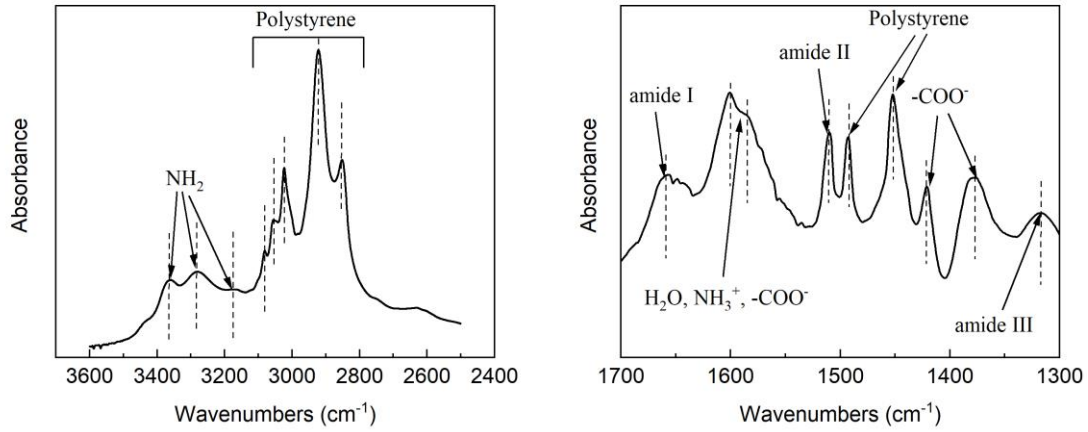

Supplementary Fig. 5. Fourier transform infrared spectroscopy (FTIR) spectra of VP OC 1065 pretreated using 25 °C air with 30% relative humidity (RH). Source data are provided as a Source Data file.

FTIR spectroscopy was used to analyze the surface species of VP OC 1065 treated with air at 25 °C and 30% relative humidity. The symmetric stretching vibration of $-COO^-$ originating from the carbamate structure was detected at 1380 and 1421 cm^{-1} [5,6]. The IR band at 1510 cm^{-1} corresponded to the N-H bending vibration and C-N stretching vibration (amide II) of carbamate species[5-7]. In addition, the asymmetric stretching vibration of $-COO^-$ and antisymmetric deformation of NH_3^+ at around 1560-1590 cm^{-1} were detected[6,7].

Generally, carbamic acid, bicarbonate, and ammonium carbamate are regarded as potential species formed on solid amine sorbents during CO_2 adsorption[8-10], with IR bands in the range of 1700-1300 cm^{-1}. Young et.al proved that the amine efficiency of Lewatit resin was not increased in the presence of moisture when CO_2 adsorption was performed at 1 bar [2]. This indicated that the bicarbonate mechanism is unlikely to occur in Lewatit resin, as the stoichiometric ratio of CO_2/amine would increase from 0.5 to 1 if the bicarbonate was formed. Previous works have also reported that the surface species shifted from carbamic acid to ammonium carbamate for amine-grafted materials in the presence of water[10-12]. Thus, we speculate that the resin primarily adsorbs atmospheric CO_2 at 25 °C and 30% RH via a carbamate pathway.

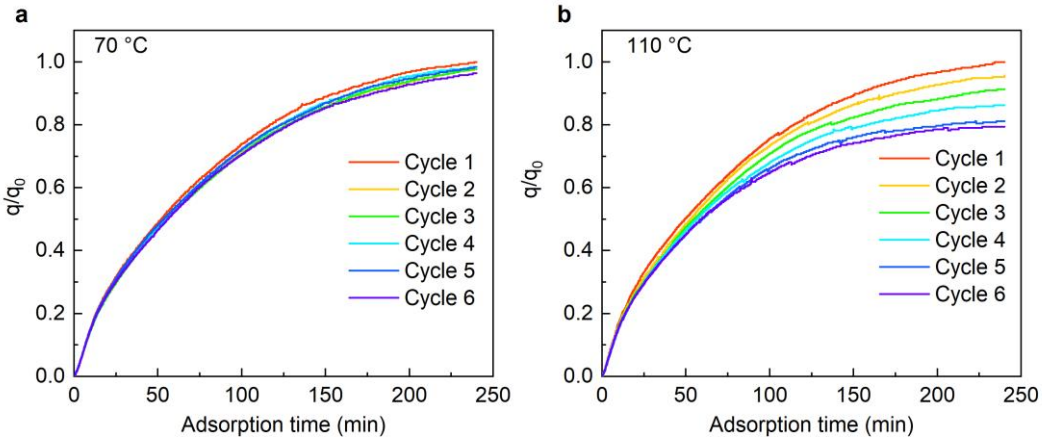

Supplementary Fig. 6. Cyclic CO_2 adsorption capacity of VP OC 1065 regenerated under 70 °C (a) and 110 °C (b) air flows. CO_2 adsorption was performed using 30 °C dry air with 400 ppm CO_2. The CO_2 uptake of the first adsorption cycle was denoted as q_0. Source data are provided as a Source Data file.

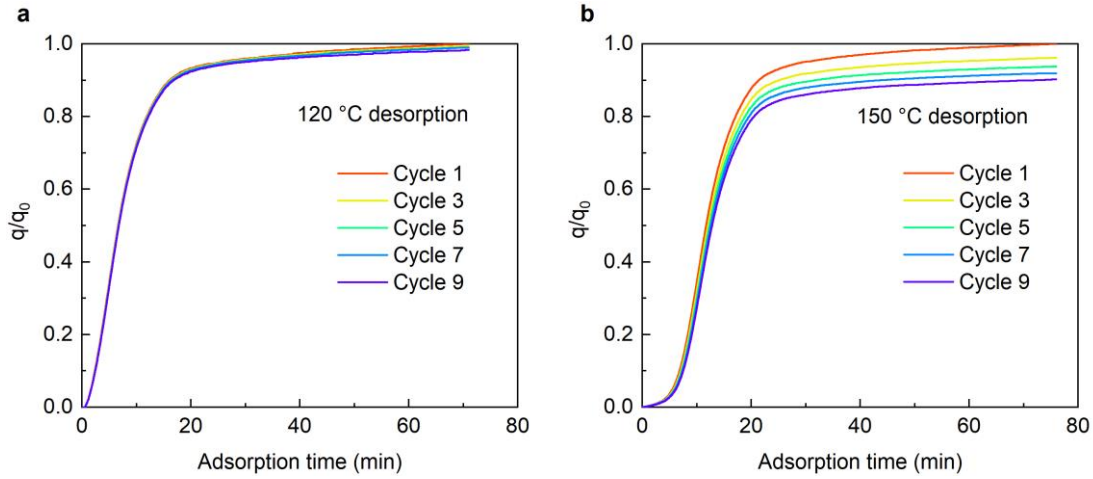

Supplementary Fig. 7. Cyclic CO_2 adsorption capacity of VP OC 1065 regenerated under 120 °C (a) and 150 °C (b) CO_2 flows. CO_2 adsorption was performed using CO_2 at 30 °C and 1 bar. The CO_2 uptake of the first adsorption cycle was denoted as q_0. Source data are provided as a Source Data file.

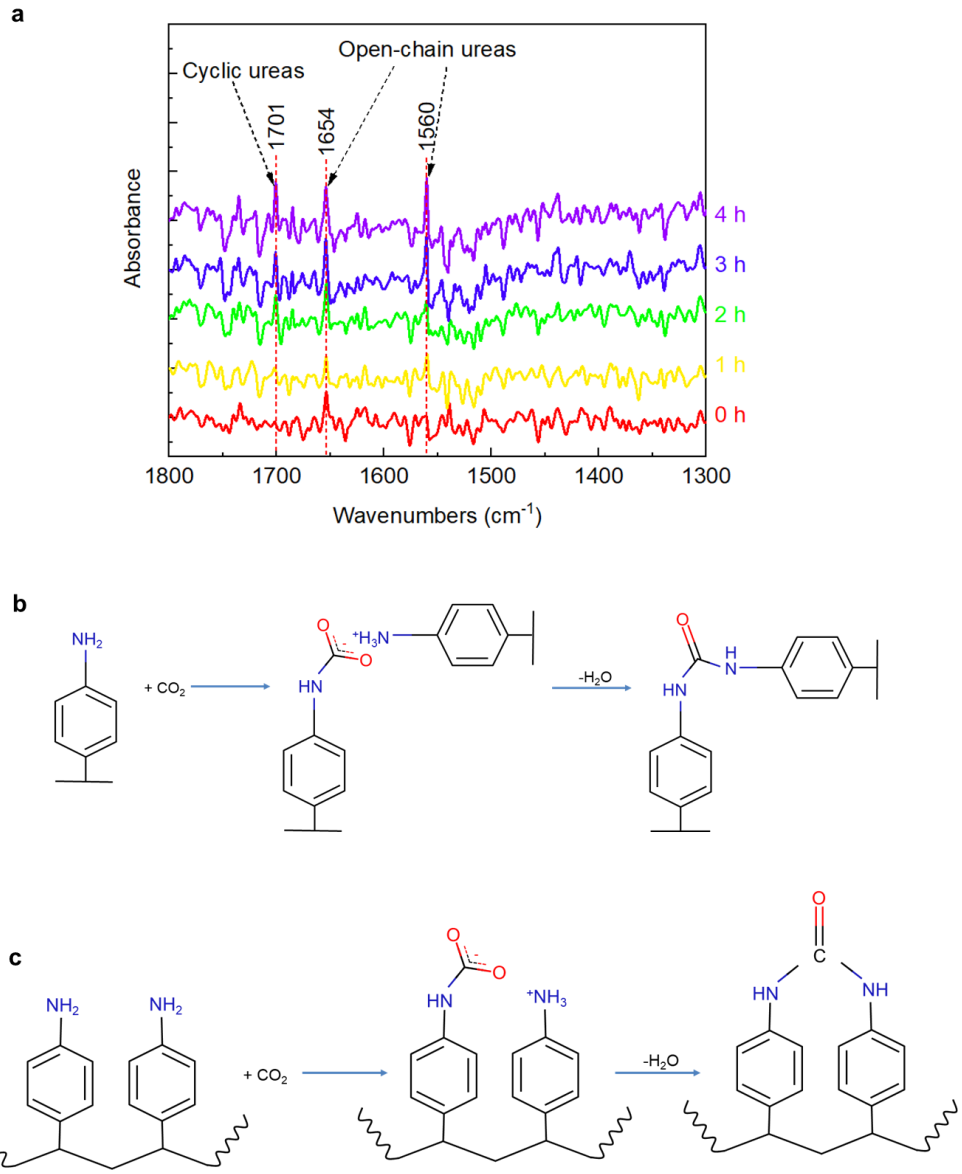

Supplementary Fig. 8. CO_2-induced deactivation mechanism analysis. (a) *In situ* FTIR spectra for VP OC 1065 after 0, 1, 2, 3, and 4 hours (bottom to top) treatment under CO_2 stream at 150 °C. **(b-c)** Proposed mechanism for **(c)** open-chain ureas formation and **(c)** cyclic ureas formation. Source data are provided as a Source Data file.

Using a CO_2 stream to treat the sample at 150 °C, the absorptance of two bands at 1560 and 1654 cm^{-1} associated with open-chain ureas gradually increased. Moreover, a new absorption band at 1702 cm^{-1} was also observed due to the formation of cyclic ureas[13,14]. Supplementary Figs. 8b and 8c illustrate the formation mechanisms of open-chain urea and cyclic urea. Specifically, two primary amine groups first react with CO_2 to form the corresponding ammonium carbamate in the CO_2 adsorption process. Subsequently, the ureas are formed through the dehydration of ammonium carbamate at 150 °C[13,14].

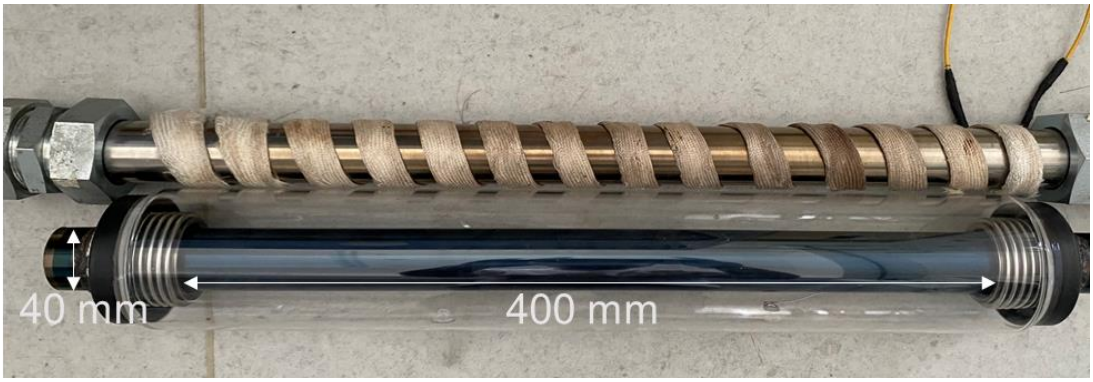

Supplementary Fig. 9. Adsorption columns for electrical heating (Top) and solar heating (Bottom).

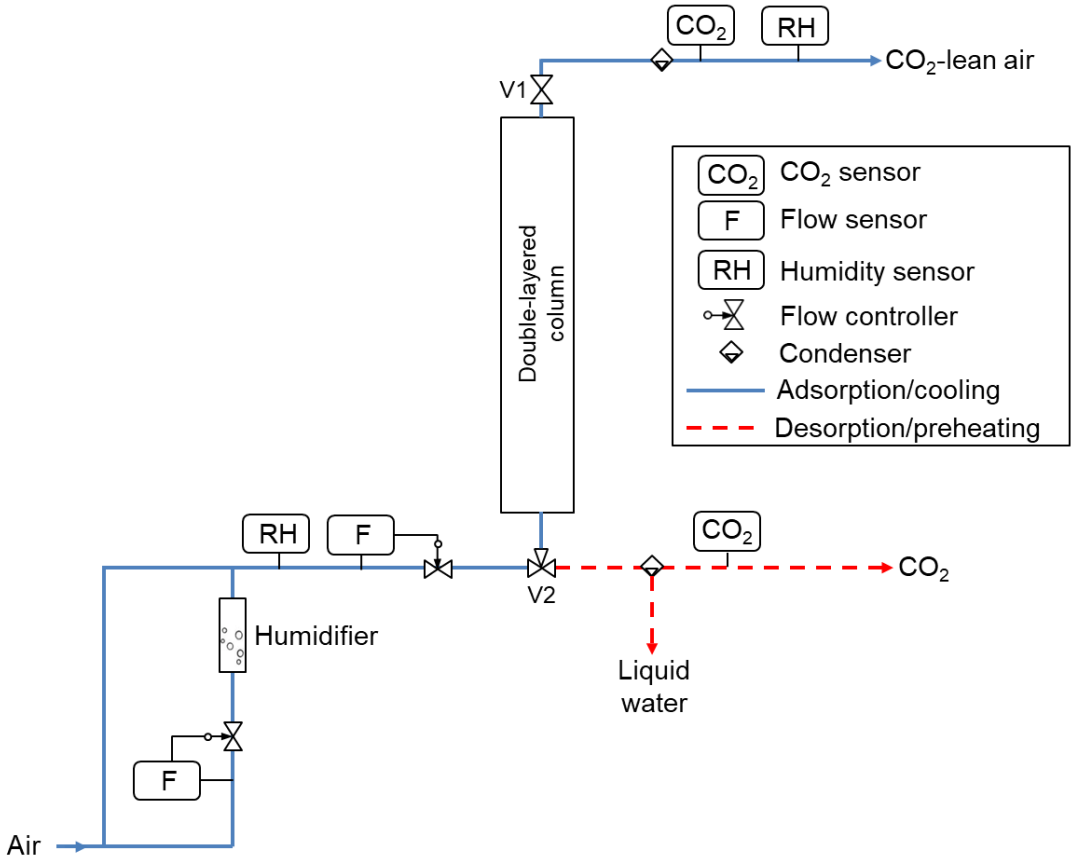

Supplementary Fig. 10. Scheme of the setup for testing cyclic performance of vapor promoted DAC.

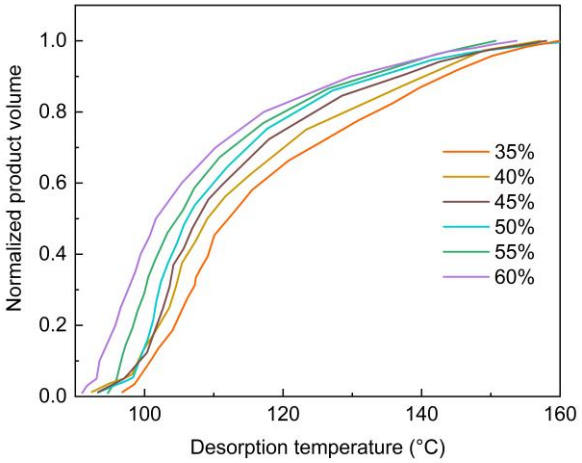

Supplementary Fig. 11. Normalized product volumes (ratios of collected product volume to final product volume) of cyclic DAC performed at various RH without *in situ* vapor purge. Adsorbent: 180 mL VP OC resin. Fresh air at 27 °C with RH ranging from 35 to 60% was used as the feed stream. Source data are provided as a Source Data file.

Without *in situ* vapor purge, the product volume and corresponding regeneration temperature were influenced by the relative humidity of the air, with higher atmospheric humidity enhancing carbon dioxide desorption.

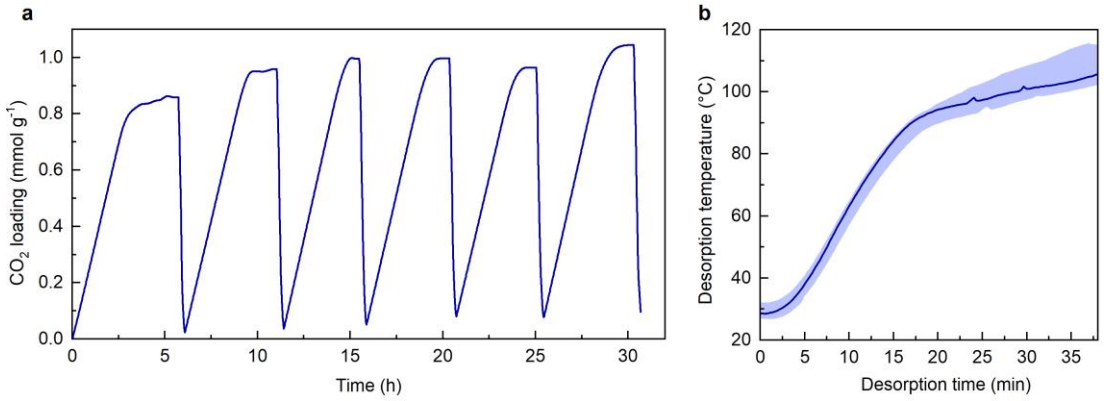

Supplementary Fig. 12. CO_2 loading (a) and desorption temperature (b) profiles in six adsorption-desorption cycles using 320 mL VP OC resin and 80 mL silica gel. Fresh air at around 27 °C with RH ranging from 45 % to 70 % was used as the feed stream which had a gas hourly space velocity (GHSV) of 5600 /h. The shaded areas indicate the variation of temperature results obtained under different relative humidities (45-70%). The solid line represents the experiment conducted under a relative humidity of 60%. Source data are provided as a Source Data file.

As shown in Supplementary Fig. 12b, the desorption temperature profile of VPD exhibited two distinct stages, corresponding to the preheating and desorption steps. Specifically, the temperature initially increased from room temperature to 90 °C, after which it stabilized or gradually increased to around 110 °C. This behavior can be attributed to the consumption of thermal energy by the desorption of CO_2 and H_2O in the desorption step. Wurzbacher et.al also reported a similar temperature evolution in the sorbent bed center during TVSA processes using solid amine materials[15].

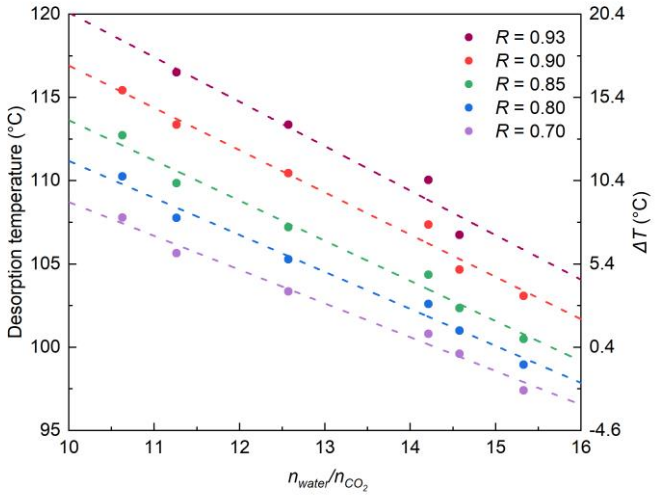

Supplementary Fig. 13. To achieve regeneration efficiency *R* ranging from 0.70 to 0.93, the corresponding desorption temperature as a function of the molar ratio of equilibrium loading of adsorbed water to CO_2 (n_{water}/n_{CO2} at the end of adsorption step). The dashed lines represent the linear fitting results. The right y-axis shows the required temperature difference (ΔT) between the desorption temperature (T_{de}) and the boiling point of water (T_{bp}) at 1 bar, with ΔT calculated as T_{de} minus T_{bp}. Source data are provided as a Source Data file.

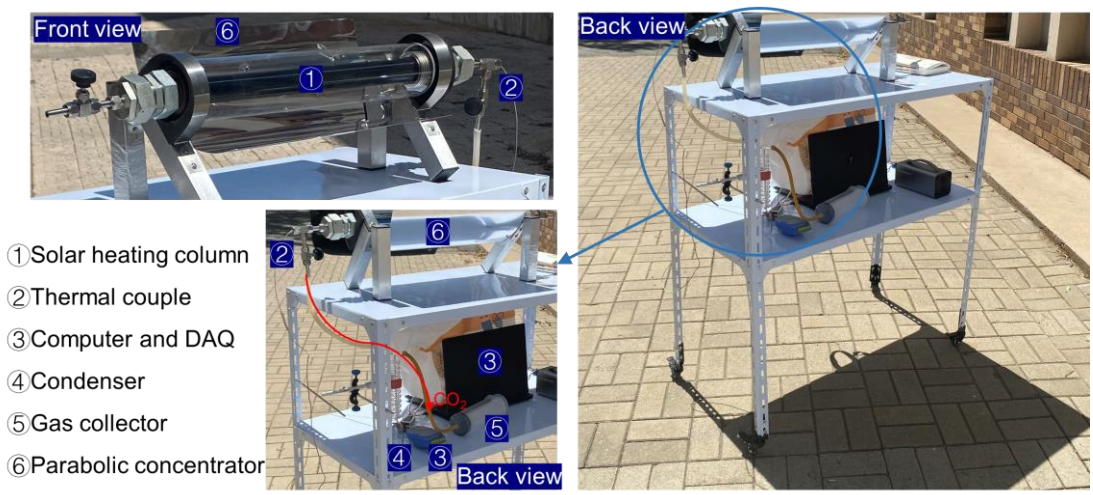

Supplementary Fig. 14. Solar-powered DAC prototype for high purity CO_2 and water production from the air.

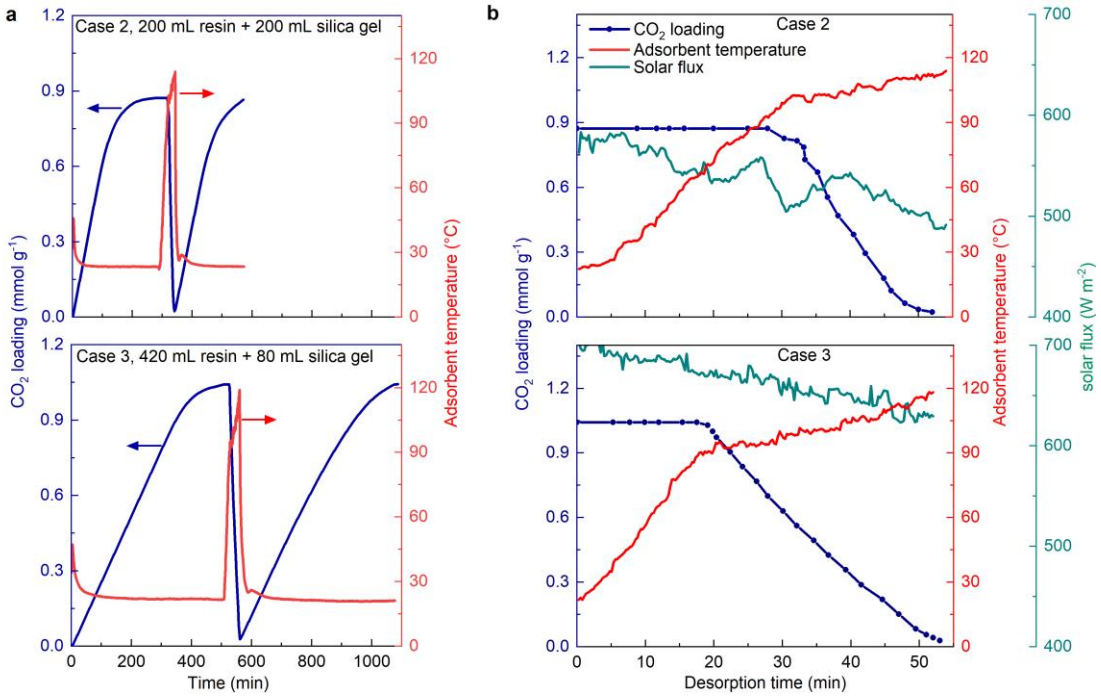

Supplementary Fig. 15. Performance of solar-powered VPD prototype for DAC with different volume fractions of resin. Solar-powered DAC with different adsorbent volumes was tested under varying weather conditions, GHSV, and humidities in Tianjin China (39°06'32.9"N 117°10'11.1"E) during May 2022. Case 2: 200 mL resin and 200 mL silica gel, at 40% RH and a gas hourly space velocity GHSV of 6000 /h. Case 3: 420 mL resin and 80 mL silica gel, at 57% RH and a GHSV of 3000 /h. Case 1, using 320 mL resin and 80 mL silica gel, performed at 56% RH and a GHSV of 3750 /h, is described in Fig. 6. **(a)** CO_2 loading and adsorbent temperature profiles during the adsorption-desorption cycles for Cases 2 and 3. **(b)** CO_2 loading, adsorbent temperature, and solar flux profiles during the solar-powered regeneration stage for Cases 2 and 3. Source data are provided as a Source Data file.

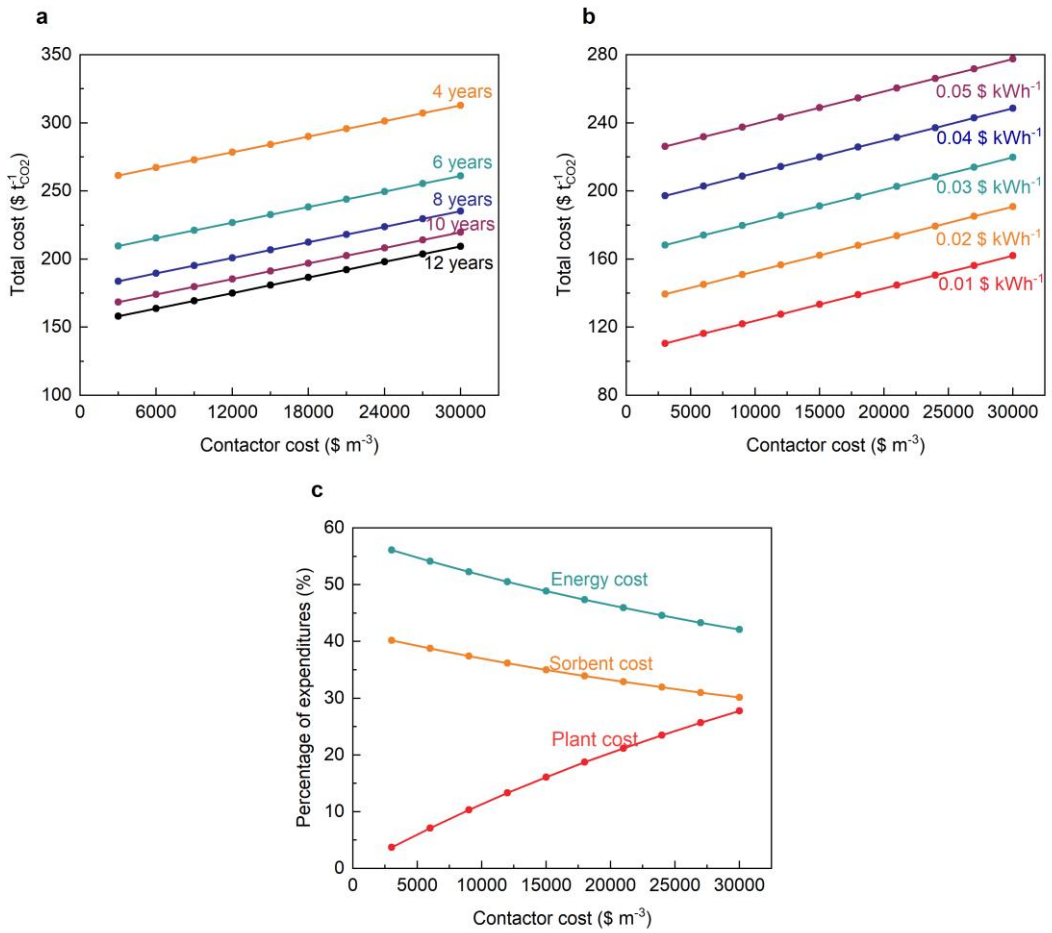

Supplementary Fig. 16. Total cost of vapor-promoted DAC process under various contactor costs. (a) The influence of adsorbent lifetime on the total cost when the heat cost is 0.03 $ kWh^{-1}. (b) The effect of heat costs on the total cost, with sorbent lifetime fixed at 10 years. (c) Percentage of different expenditures for a heat cost of $0.03 kWh^{-1} and an adsorbent life of 10 years. The solid lines are guides to the eye. Source data are provided as a Source Data file.

Supplementary Table 1. Dual-site Langmuir model parameters of CO_2 adsorption on Lewatit resin.

Parameter	Value
q_1 (mmol g^{-1})	1.94
q_2 (mmol g^{-1})	1.06
$K_{0,1}$ (Pa^{-1})	1.11×10^{-15}
$K_{0,2}$ (Pa^{-1})	1.84×10^{-13}
$-\Delta H_{ads,1}$ (kJ mol^{-1})	75.6
$-\Delta H_{ads,2}$ (kJ mol^{-1})	51.6

Supplementary Table 2. Parameters used for evaluating energy consumption in vapor-promoted desorption process.

Parameter	Value
$C_{p,resin}$ (J kg^{-1} K^{-1})	1580[16]
$C_{p,silica}$ (J kg^{-1} K^{-1})	921[17]
C_{p,CO_2} (J kg^{-1} K^{-1})	2000[18]
C_{p,H_2O} (J kg^{-1} K^{-1})	4184
h_{des,CO_2} (kJ mol^{-1})	75.6
h_{des,H_2O} (kJ mol^{-1})	44[19]

Supplementary Table 3. Performance of reported experimental DAC works performed using different adsorption processes. The working capacities (W_c), desorption temperatures (T_{de}), desorption pressures (P_{de}), energy consumptions, CO_2 product purities, and total costs of the reported processes are listed and compared with the VPD process.

Sorbent	Process	W_c (mmol g^{-1})	T_{de} (°C)	P_{de} (bar)	Q_{re} [a] (MJ kg^{-1}_{CO2})		Purity	Cost ($ t^{-1}_{CO2})
					Q_{th} [b]	Q_e [c]		
VP OC 1065	VPD	1.0	105	1	10.4	0	98%	111-313
Sorbent-coated carbon fibers[20]	ETSA[d]	0.54	110	0.3	0	7.2	82%	160
VP OC 1065[21]	TVSA	0.38	116	0.5	12.4	0.54	-[e]	-
VP OC 1065[21]	STVSA	0.77	116	0.5	14.5	0.54	-	-
PEI-silica[22]	TSA	1.14	130	1	6.6	0	<7%	152
APDES-NFC[23]	TVSA	0.5	95	0.05	14.5	0.28	94%	-
Anion exchange resin[24]	pH-swing	1.17	25	1	0	12.2	95%	-

[a] Energy consumption for sorbent regeneration.

[b] Thermal energy consumption for sorbent regeneration.

[c] Electricity consumption for sorbent regeneration.

[d] Electrically driven temperature swing adsorption.

[e] Not reported.

Supplementary Table 4. Parameters used for evaluating the total cost of the vapor-promoted DAC process.

Parameter	Value
r_{ac} ($ m^{-3})	3000-30000[1]
$V_{f,resin}$	0.8
P_r (kg h^{-1} m$^{-3}_{resin}$)	3.8
a_p (year)	20[1]
r_{resin} ($ m^{-3})	20000
r_{silica} ($ m^{-3})	1500
a_s (year)	4-12
c_{th} ($ kWh^{-1})	0.01-0.05[1]
Q_{re} (MJ kg$^{-1}_{CO2}$)	10.4
c_{el} ($ kWh^{-1})	0.1[1]
E_{blower} (MJ kg$^{-1}_{CO2}$)	0.5[1,25]

Supplementary References

1. Sabatino, F., Grimm, A., Gallucci, F., van Sint Annaland, M., Kramer, G.J. & Gazzani, M. A comparative energy and costs assessment and optimization for direct air capture technologies. *Joule* 5, 2047-2076 (2021).
2. Young, J., García-Díez, E., Garcia, S. & van der Spek, M. The impact of binary water-CO_2 isotherm models on the optimal performance of sorbent-based direct air capture processes. *Energ. Environ. Sci.* 14, 5377-5394 (2021).
3. Veneman, R., Zhao, W., Li, Z., Cai, N. & Brilman, D.W.F. Adsorption of CO_2 and H_2O on supported amine sorbents. *Energy Procedia* 63, 2336-2345 (2014).
4. Buijs, W. & de Flart, S. Direct air capture of CO_2 with an amine resin: A molecular modeling study of the CO_2 capturing process. *Ind. Eng. Chem. Res.* 56, 12297-12304 (2017).
5. Danon, A., Stair, P.C. & Weitz, E. FTIR study of CO_2 adsorption on amine-grafted SBA-15: Elucidation of adsorbed species. *The Journal of Physical Chemistry C* 115, 11540-11549 (2011).
6. Bacsik, Z., Ahlsten, N., Ziadi, A., Zhao, G., Garcia-Bennett, A.E., Martín-Matute, B. & Hedin, N. Mechanisms and kinetics for sorption of CO_2 on bicontinuous mesoporous silica modified with n-propylamine. *Langmuir* 27, 11118-11128 (2011).
7. Bacsik, Z., Atluri, R., Garcia-Bennett, A.E. & Hedin, N. Temperature-induced uptake of CO_2 and formation of carbamates in mesocaged silica modified with n-propylamines. *Langmuir* 26, 10013-10024 (2010).
8. Alesi, W.R. & Kitchin, J.R. Evaluation of a primary amine-functionalized ion-exchange resin for CO_2 capture. *Ind. Eng. Chem. Res.* 51, 6907-6915 (2012).
9. Hahn, M.W., Steib, M., Jentys, A. & Lercher, J.A. Mechanism and kinetics of CO_2 adsorption on surface bonded amines. *The Journal of Physical Chemistry C* 119, 4126-4135 (2015).
10. Flaig, R.W., Osborn Popp, T.M., Fracaroli, A.M., Kapustin, E.A., Kalmutzki, M.J., Altamimi, R.M., Fathieh, F., Reimer, J.A. & Yaghi, O.M. The chemistry of CO_2 capture in an amine-functionalized metal-organic framework under dry and humid conditions.

J. Am. Chem. Soc. 139, 12125-12128 (2017).

11. Forse, A.C., Milner, P.J., Lee, J., Redfearn, H.N., Oktawiec, J., Siegelman, R.L., Martell, J.D., Dinakar, B., Zasada, L.B. & Gonzalez, M.I., et al Elucidating CO_2 chemisorption in diamine-appended metal-organic frameworks. *J. Am. Chem. Soc.* 140, 18016-18031 (2018).
12. Mafra, L., Čendak, T., Schneider, S., Wiper, P.V., Pires, J., Gomes, J.R.B. & Pinto, M.L. Structure of chemisorbed CO_2 species in amine-functionalized mesoporous silicas studied by solid-state NMR and computer modeling. *J. Am. Chem. Soc.* 139, 389-408 (2017).
13. Sayari, A., Belmabkhout, Y. & Da Na, E. CO_2 deactivation of supported amines: Does the nature of amine matter? *Langmuir* 28, 4241-4247 (2012).
14. Sayari, A., Heydari-Gorji, A. & Yang, Y. CO_2-induced degradation of amine-containing adsorbents: Reaction products and pathways. *J. Am. Chem. Soc.* 134, 13834-13842 (2012).
15. Wurzbacher, J.A., Gebald, C. & Steinfeld, A. Separation of CO_2 from air by temperature-vacuum swing adsorption using diamine-functionalized silica gel. *Energ. Environ. Sci.* 4, 3584-3592 (2011).
16. Sonnleitner, E., Schöny, G. & Hofbauer, H. Assessment of zeolite 13X and Lewatit® VP OC 1065 for application in a continuous temperature swing adsorption process for biogas upgrading. *Biomass Conversion and Biorefinery* 8, 379-395 (2018).
17. Robens, E. & Wang, X. Investigation on the isotherm of silica gel+water systems. *J. Therm. Anal. Calorim.* 76, 659-669 (2004).
18. Wurzbacher, J.A., Gebald, C., Brunner, S. & Steinfeld, A. Heat and mass transfer of temperature-vacuum swing desorption for CO_2 capture from air. *Chem. Eng. J.* 283, 1329-1338 (2016).
19. Demir, H., Mobedi, M. & Ülkü, S. Microcalorimetric investigation of water vapor adsorption on silica gel. *J. Therm. Anal. Calorim.* 105, 375-382 (2011).
20. Lee, W.H., Zhang, X., Banerjee, S., Jones, C.W., Realff, M.J. & Lively, R.P. Sorbent-

coated carbon fibers for direct air capture using electrically driven temperature swing adsorption. *Joule* 7, 1241-1259 (2023).

21. Bos, M.J., Pietersen, S. & Brilman, D.W.F. Production of high purity CO_2 from air using solid amine sorbents. *Chemical Engineering Science: X* 2, 100020 (2019).
22. Zhang, W., Liu, H., Sun, C., Drage, T.C. & Snape, C.E. Capturing CO_2 from ambient air using a polyethyleneimine-silica adsorbent in fluidized beds. *Chem. Eng. Sci.* 116, 306-316 (2014).
23. Wurzbacher, J.A., Gebald, C., Piatkowski, N. & Steinfeld, A. Concurrent separation of CO_2 and H_2O from air by a temperature-vacuum swing adsorption/desorption cycle. *Environ. Sci. Technol.* 46, 9191-9198 (2012).
24. Shu, Q., Haug, M., Tedesco, M., Kuntke, P. & Hamelers, H.V.M. Direct air capture using electrochemically regenerated anion exchange resins. *Environ. Sci. Technol.* 56, 11559-11566 (2022).
25. Zhu, X., Ge, T., Yang, F. & Wang, R. Design of steam-assisted temperature vacuum-swing adsorption processes for efficient CO_2 capture from ambient air. *Renewable and Sustainable Energy Reviews* 137, 110651 (2021).